SUPPLEMENTARY APPENDIX

for

Finerenone added to RAS/SGLT2 blockade for chronic kidney disease in Alport syndrome. Results of a randomized controlled trial in *Col4a3*-/- mice.

by

Zhihui Zhu, Karoline AT Rosenkranz, Yoshihiro Kusunoki, Chenyu Li, Martin Klaus, Oliver Gross, Maria-Lucia Angelotti, Giulia Antonelli, Luigi Cirillo, Paola Romagnani, Nassim Bouteldja, Alireza Vafaei Sadr, Roman D. Bülow, Peter Boor, Hans-Joachim Anders

LIST

Supplementary file 1 Material and methods

Inclusion criteria, exclusion criteria, and intervention

Inclusion criteria were as follows: Male and female mice, six weeks of age. The exclusion criteria were the following: a score ≥ 2 for more than 6h during animal welfare surveillance; exposure to any other drug during the study period, e.g., treatment requested by the veterinarian for skin wounds; any sign of infection; pregnancy; signs of drug intolerance (anaphylactic reactions).

In our study, mice were treated with food admix of either a) vehicle, b) 10 mg/kg ramipril, c) 10 mg/kg ramipril plus 30 mg/kg empagliflozin, or d) 10 mg/kg ramipril plus 30 mg/kg empagliflozin plus 10 mg/kg finerenone. We based the dose of each drug on what has been used before in numerous mouse studies in the literature [1-4]. The composition of ramipril mixed with food was 0.05 mg of ramipril per gram of food. The composition of empagliflozin mixed with food was 0.15 mg of empagliflozin per gram of food. The composition of finerenone mixed with food was 0.05 mg of finerenone per gram of food. The different types of food preparations were marked by different food colors starting from 6 weeks of age for 8 weeks.

Randomization, blinding, and grouping

A stratified randomization method was used using the following R code of “Package blockrand”:

```
library(blockrand)

male<-blockrand(n=40,num.levels=4,levels=c("A","B","C","D"),id.prefix='M',
block.prefix='M',stratum='Male')

female<-blockrand(n=40,num.levels=4,levels=c("A","B","C","D"),id.prefix='F',
block.prefix='F',stratum='Female')

my.study <- rbind(male,female)


p=plotblockrand(my.study,'mystudy.pdf',
```

```
top=list(text=c('Combination therapy in Mice with Alport Syndrome',
'Mouse ID: %ID%','Treatment: %TREAT%',
'from Cage: ',"Ear mark:","DOB:","Experiment date:","","Signature:"),
col=c('black','black','black','red','black','black','black','black','black','black'),
font=c(1,1,1,4,1,1,1,1,1,1)),

middle=list(text=c("Combination therapy in Mice with Alport Syndrome",
"Sex: %STRAT%","Mouse ID: %ID%"),
col=c('#80afd2','#6594c4','#4575b4'),font=c(1,2,3)),

bottom="Demo",
cut.marks=TRUE)

https://cran.r-project.org/web/packages/blockrand/index.html
```

Male and female mice who met the inclusion and not exclusion criteria were randomized in a 1:1:1:1 ratio into control group and treatment groups. Mice were not aware of their grouping, and the researchers conducting the end point evaluation were blinded to the groupings.

Primary and secondary endpoints

The primary end point of this study was the overall survival. Animal welfare scoring was performed daily by personnel blinded to treatment groups. Upon reaching a predefined score (supplementary file 3), animals were sacrificed, and the time point was recorded as the day of uremic death. Tissues and biosamples were harvested to validate end-stage kidney disease as the cause of demise. The secondary end point was the makers of kidney excretory function (GFR, proteinuria) and histomorphological parameters of the kidney in a subgroup of animals.

Measurement of GFR, proteinuria, serum BUN, creatinine (Cr), potassium, phosphate, and glucose

GFR was measured in conscious and unrestricted mice before the onset of treatment and several

subsequent time points using a transcutaneous detector system for FITC-Sinistrin clearance kinetics (Mannheim Pharma & Diagnostics GmbH, Germany) as described [5,6]. Urine samples were collected every 2 weeks for the estimation of creatinine (DiaSys Diagnostic Systems, Holzheim, Germany) and albumin (Bethyl Laboratories, Montgomery, MD). The levels of BUN and Cr in mouse serum were measured using the enzymatic method (Urea FS, Diasys, Germany) and the Jaffe method (Creatinine FS Diasys, Germany), respectively. Urinary glucose was measured suing hexokinase/glucose-6-phosphate dehydrogenase method (Cayman Chemical, Michigan, USA). Urinary glucose-to-creatinine ratio (UGCR) was calculated as (mg/mg) = urine glucose (mg/dL)/urine creatinine (mg/dL). All ELISA and colorimetric assays followed the manufacturer's protocols. Kalium and phosphate were tested in SYNLAB Munich.

Histology, immunostaining, immunofluorescence, and quantitative analysis

Transverse kidney sections were then sectioned at 3 μm and stained with Periodic Acid Schiff (PAS), Picro-Sirius Red, Alpha smooth muscle actin (αSMA), Wilms tumor 1 (WT-1), F4/80, TdT-mediated dUTP-biotin nick-end labeling (TUNEL) according to standard protocols. Images of the sections were scanned by light microscopy, and quantitative analysis was performed by the software of Photoshop and OpenCV. Histopathology scoring was performed by two blinded independent renal pathologists. The scores were defined by the percentage of tissue exhibiting pathological changes out of the total reviewed area. Multiple fields were evaluated for each sample, and the mean value was used as the final score. The methods of deep learning-based model for the automated segmentation of major kidney structures, deep learning morphometry analysis of WT1 stained immunohistochemistry slides, and confocal 3D reconstruction were shown in supplementary file 4.

RNA-Sequencing

RNA was extracted from the kidneys of four *Col4a3*-/- mice groups and WT mice at the age of 8.5 weeks. The library construction and sequencing were performed by Beijing Genomics Institute (BGI) using DNBSEQ (G400) platform. The RNAs were subjected to 100-bp paired-end sequencing. The bioinformatics workflow, which included data filtering, mapped transcript prediction, analysis of

differential gene expression and gene ontology, was carried out in accordace with the protocols of HISAT2 [7], SAMtools [8], featureCounts [9], eisaR [10], and clusterProfiler [11]. The full data can be found at Gene Expression Omnibus (GEO) (Accession number: GSE226353).

Transcriptome analysis

Total RNA was isolated using an RNA extraction kit (Life Technologies, Darmstadt, Germany) according to the manufacturer´s instructions, and RNA quality was assessed using agarose gels. After the isolation of RNA, cDNA was generated using reverse transcriptase (Superscript II; Invitrogen, Carlsbad, CA). SYBR Green Dye detection system was used for quantitative real-time PCR on Light Cycler 480 (Roche, Mannheim, Germany) using 18s rRNA as a housekeeping gene. Gene-specific primers blasted with ensemble-BLAST and NCBI primer-BLAST (Metabion, Martinsried, Germany) were used as listed in supplementary file 5. Non-template controls consisting of all used reagents were negative for target and housekeeping genes. To reduce the risk of false positive crossing points, the high confidence algorithm was used. The melting curve profiles were analyzed for every sample to detect eventual unspecific products or primer dimers as housekeeping gene 18s RNA was taken.

Statistical analysis

Data are presented as mean with SD or as boxplot statistics. Before statistical analysis, data were analyzed for normal distribution by checking the distribution of the data against the expected normal distribution with a quantile-quantile (Q-Q) plot and confirmation with the Shapiro–Wilk test. We tested normally distributed data for statistically significant differences via ANOVA, and post hoc Tukey's correction was used for multiple comparisons. Non-normally distributed data were compared using Wilcoxon signed-rank testing or Kruskal–Wallis testing with post hoc Dunn's test correction for multiple comparisons. Survival was plotted on Kaplan–Meier curves, and comparisons between groups were evaluated using log-rank tests. Correlation coefficient was calculated by Point-biserial algorithm. A value of $p<0.05$ was considered to indicate statistical significance. All statistical analyses were performed with R (3.5.3).

Supplementary file 2

PRECLINICAL PROTOCOL LMU

Date: 20 October 2021

Study Synopsis

Study Number

2021-COMB-CKD-001

Title of the Study

A Preclinical, Randomized, Double-Blind, Placebo-Controlled Study to Evaluate the Efficacy and Safety of Combination Therapy to target CKD Progression in Adult Mice

Preclinical Development Phase

Academic research, single centre study

Coordinating Center

Department of Medicine IV, Hospital of the Ludwig-Maximilians-University, Renal Division, Munich, Germany

Participating Center

Department of Medicine IV, Hospital of the Ludwig-Maximilians-University, Renal Division, Munich, Germany

Objectives

• To evaluate the efficacy of dual Ramipril-Empagliflozin therapy versus Ramipril monotherapy on CKD progression in adult Alport mice.

• To assess the safety and tolerability of triple Ramipril-Empagliflozin-Finerenone therapy versus dual Ramipril-Empagliflozin therapy on CKD progression in adult Alport mice.

Inclusion Criteria

Male and female 129-*Col4a3*^{tm1Dec}-/- mice, six weeks of age.

Exclusion Criteria

Mice will be excluded from participating in the study if they meet any of the following exclusion criteria:

• A welfare score 4 or score ≥ 2 for more than 6h during animal welfare surveillance.

• Exposure to any other drug during the study period, e.g., treatment requested by the veterinarian for skin wounds.

• Any sign of infection.

• Pregnancy.

• Signs of Ramipril, Empagliflozin, Finerenone intolerance (anaphylactic reactions).

Intervention

In our study, mice were treated with food admix of either a) vehicle, b) 10 mg/kg ramipril, c) 10 mg/kg ramipril plus 30 mg/kg empagliflozin, or d) 10 mg/kg ramipril plus 30 mg/kg empagliflozin plus 10 mg/kg finerenone. The different types of food preparations were marked by different food colors starting from 6 weeks of age for 8 weeks.

Study Design and Schedule:

This is a preclinical, randomized, double-blind, placebo-controlled study to evaluate the efficacy and safety of combination therapy to target CKD progression in adult mice. The randomization of all eligible mice will be stratified by their induction regimen. Alport mice will be dosed with a vehicle, Ramipril, Ramipril-Empagliflozin, or Ramipril-Empagliflozin-Finerenone once daily with the study agent by gastric tube administration for eight weeks.

The primary efficacy endpoint will be the mean overall survival.

The Secondary endpoints will be renal function, proteinuria, histomorphological parameters of kidney atrophy. Renal function assessments will be based on measured glomerular filtration rate (mGFR) at study sites where the necessary experience and hardware are available. In addition, serum markers of renal excretory function (serum creatinine/SCr and blood urea nitrogen/BUN levels) will be measured.

A safety analysis will include animal welfare scoring in all animals and a histomorphological analysis of non-renal tissues in a subset of animals.

Experimental Animals, Housing, and Husbandry

129-*Col4a3*^{tm1Dec}-/- mice with spontaneous CKD (Alport nephropathy) will be used in this study and bred in an in-house colony. All mice will be kept under pathogen-free conditions in a 12-hour light and dark cycle with free access to food and water. Enrichment will be provided as per local regulatory requirements. Health status, cleaning, beddings, water, and food supply with standard chow will be according to our center's local standard operating procedures.

Primary Efficacy Endpoint

• Mean overall survival.

Major Secondary Endpoints

• Markers of renal excretory function (mGFR, SCr, BUN).

• Histomorphological parameters of the kidney in a subgroup of animals.

• Safety analysis: Animal welfare scoring (all animals), histomorphological analysis of non-renal tissues (subset of animals).

Sample Size Calculation

Group comparisons are determined about the (kidney) survival time, defined as achieving a stress score greater than 2 for more than 6 hours. A comparison is made with vehicle-treated animals. A minimum survival time of 60 days is assumed here. The expected median duration in the control group is 70 days. An extension to 85 days is clinically relevant. It can be assumed that there will be no failures up today 60. The log-rank test is used as a statistical test. This corresponds to a clinically relevant hazard coefficient of (85-60) / (70-60) = 2.5. With an error of the first type of α= 0.05 and an error of the second type β= 0.2, the sample size is n = 20 per group. The use of a two-sided test is necessary because it cannot be ruled out that individual therapy groups also lead to a shortening of the (kidney) survival time, which would be significant since all test substances are already in clinical use elsewhere.

Randomized and Double-Blind Strategy

We use the idea of "Stratified randomization" to achieve randomization. We use the function to create random assignments for clinical trials (or any experiment where the subjects come one at a time). The randomization is done within blocks so that the balance between treatments stays close to equal throughout the trial. (see the figure below)

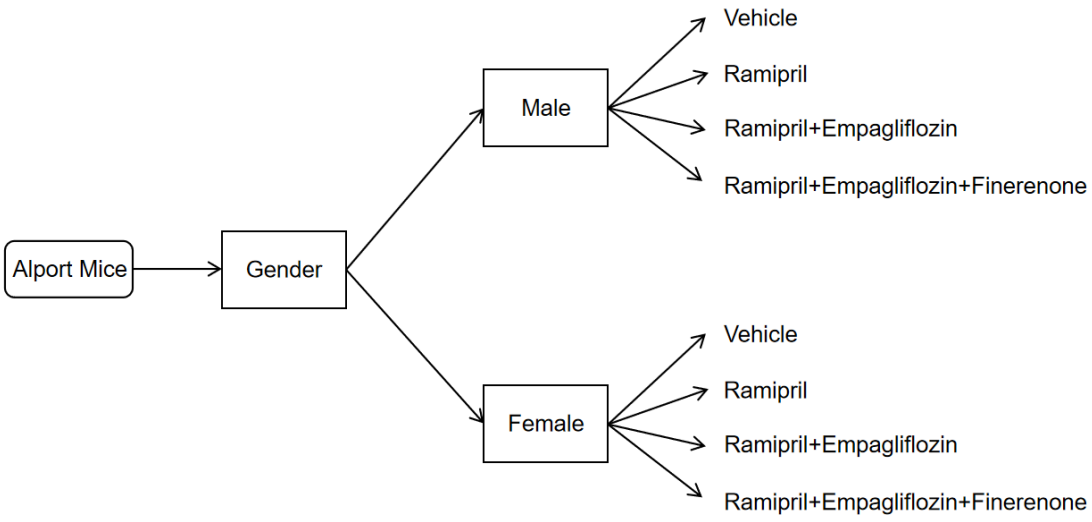

An external person, otherwise not involved in this project, will keep the Random Card and Form and prepare drug stocks labeled as A, B, C or D, while the researchers performing the study remain blinded to what treatment is ABCD. For each new mouse, the external person will give a random card

informing about the type of treatment labeled as either A, B, C or D. Only upon finishing all the experiments and after analyzing the results, the researchers will be unblinded for ABCD. Only the external person knew which food color represented which treatment. The code was locked in a safe and the envelope was opened by all participants after the end of the study and the completed blinded analysis.

Safety Endpoints and Analysis

Welfare scoring was used for welfare analysis. Sporadic kidney histology done on mice at the end of life confirmed that death was due to kidney failure.

Study Schematic

The study schematic is shown in the figure below:

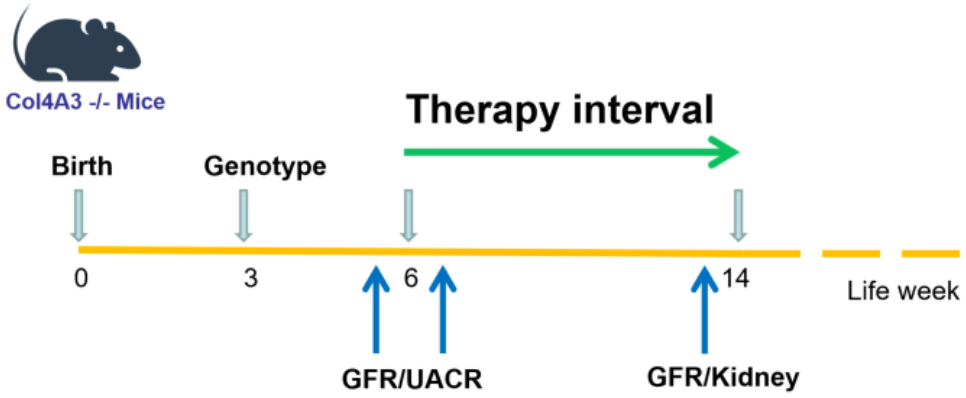

Supplementary file 3

Animal welfare surveillance

No alterations	**Mildly altered (1 point)**	**Moderately altered (2 points)**	**Severely altered (4 points)**
Shiny, clean fur Builds nest Social interactions Reacting to stimulus Normal motions Exploratory behavior GFR＞150 ul/min	Weight loss <10% Partially pilo erection Dampened but reactive Transient bent back Transients tremor Transient abnormal respiration Transient wet wound GFR 50-150ul/min	Weight loss <15% Permanent piloerection Dampened on provocation Intermittent bent back Repeated abnormal breathing Intermittent tremor Transient exhaustion· Redness, swelling at the injection site GFR＜50 µl/min	Weight loss >15% Moderate-severe dehydration Not reactive to stimuli Persistent back bending Persistent abnormal breathing Persistent tremor Convulsions Persistent exhaustion Self-destructive injuries Self-isolation

• “transient”: only one time detected in two subsequent checks

• “intermittent”: in three subsequent checks 1. Timepoint: yes; 2. Timepoint: no; 3. Timepoint: yes.

• “repeated”: at two-time points.

• “persistent”: > 2-time points.

• “moderate dehydration”: piloerection and possible cause of mild weight loss. Both 2 points. Give volume (s.c. NaCl 0.9 % 0.2 - 0.4 mL at max. volume 10 mL/kg in single injection site).

• Termination (cervical dislocation) once 4 points have been reached in summation or at the one-time point.

• A sum score of 2 or 3 points: repeat assessment after 6 and 12 h. Worsening should lead to consultation with a veterinarian.

Supplementary file 4

Histology, immunostaining, immunofluorescence, and quantitative analysis

The detailed pathological scoring criteria for tubulointerstitial fibrosis (from Picro-Sirius Red-stained kidney sections) and for glomerulosclerosis and tubular atrophy (from PAS-stained kidney sections) were 0 (no lesions), 1 (lesions < 25%), 2 (lesions 25-50%), 3 (lesions > 50%). The total score is the sum of the interstitial fibrosis score, glomerulosclerosis score, and tubular atrophy score. For the Sirius red staining, kidney fibrosis was quantified by evaluating the percentage of collagen (red) in tissue sections. For the αSMA staining, sections were stained with rabbit anti-mouse αSMA antibody by immunohistochemistry method (1:500, Dako, Hamburg, Germany). Photoshop software was used to calculate the percentages of SMA-positive nuclei. For the WT-1 staining, sections were stained with anti-mouse WT-1 antibody by immunohistochemistry method (1:200, Santa Cruz Biotechnology). 15-20 glomeruli in the cortex and with a vascular pole or urinary pole were chosen. WT-1 positive cells at the junction between the capsule and tufts were excluded. Results were reported as positive cells per glomerulus. For the F4/80 staining, sections were stained with antibody (CI-A3-A) by immunohistochemistry method (1:100, Novusbio NB600-404). Slides were scanned using a microscope with a total magnification of 200 × and then analyzed using Photoshop software. The number of F4/80 positive and total pixels per chip was measured, and their ratio was calculated. For the TUNEL staining, TUNEL Assay Kit-FITC (ab66108) was used to identify dead cells in the kidney. Slides were evaluated with a Fluorescence microscope and subsequently photographed. TUNEL-positive cells were assessed using Photoshop software.

Images of the sections were scanned by light microscopy, and quantitative analysis was performed by the software of Photoshop and OpenCV. Histopathology scoring was performed by two independent renal pathologists in a blinded fashion. The scores were defined by the percentage of tissue exhibiting pathological changes out of the total reviewed area. Multiple fields were evaluated for each sample, and the mean value was used as the final score.

Segmentation and feature extraction

We applied a deep learning-based model for the automated segmentation of major kidney structures including glomeruli, tufts, arteries, their lumina, and tubules, from murine histology [12,13]. The segmentation pipeline consisted of multiple steps. First, Otsu's threshold method was used to automatically detect the tissue in the WSI. Second, the detected tissue was resampled into 0.3372 um pixel size and, third, segmented by the CNN in a sliding window fashion. Fourth, the predictions were post-processed by closing holes, removing very small predictions, and dilating tubular predictions. For each detected structure, we computed morphometric features. For glomeruli, we computed the following features: “glom_sizes", "glom_diameters", "glom_distance_to_closest_glom", "glom_shape_circularity", "glom_shape_eccentricity", "glom_shape_elongation", "glom_shape_solidity", "glom_tuft_sizes",

"glom_tuft_shape_circularity", "glom_tuft_shape_eccentricity", "glom_tuft_shape_elongation", "glom_tuft_shape_solidity", "glom_bowman_sizes", "glom_tufttocapsule_ratio". For tubuli and vessels, we computed: "tubule_diameters", "tubule_sizes", "artery_diameters", "artery_sizes_wall", "artery_sizes_lumen", "artery_diameters_wall", "artery_diameters_lumen", "artery_structure_distance", "interstitium_area", "tubule_area".

Staining and Scanning

We used paraffin-embedded kidney tissue fixed in formalin (FFPE-material). Sections of 1–2-µm thickness were stained with PAS and counterstained with hematoxylin. Slides were digitalized using the whole-slide scanner Aperio AT2 with the 40x objective (Leica Biosystems, Wetzlar, Germany)

Histopathology analysis

Digital scans were analyzed by an experienced nephropathologist manually scoring number of cellular crescents, number of segmentally sclerotic glomeruli and number of globally sclerotic glomeruli. In case of unclear morphology, a second experienced nephropathologist was consulted and the consensus was of the two was used for further analyses. In addition, the total number of glomeruli per slide were counted.

Optical tissue clearing and confocal 3D reconstruction

For the 3D reconstruction of the whole glomeruli and for quantification of filtration slit density, optical clearing of the kidneys was performed. Briefly, kidneys were dissected, fixed 3h in 4% PFA and incubated at 4°C in hydrogel solution (4% v/v acrylamide, 0.025% v/v bisacrylamide, 0.25% w/v VA-044 initiator, 4% PFA) for 1 day. The gel was polymerized at 37°C for 3 h, and the presence of oxygen was minimized by filling tubes to the top with hydrogel solution. Samples were removed from the hydrogel solution, immersed in clearing solution (200 mmol/l boric acid, 4% SDS, pH 8.5) and incubated at 50°C for 1 day. Kidneys were cut in 300 µm thick slices using a Vibratome and incubated at 50°C for 5 days with clearing solution changed every day. Before immunolabeling, samples were incubated in PBST (0.1% Triton-X in 1 × PBS) for 1 day. During immunolabeling, PBST was used as diluent in all steps. Samples were incubated in primary antibody for 24 h at 37°C and then washed in PBST for 4 h at 37°C followed by secondary antibody incubation for 24 h at 37°C and washed for 4 h at 37°C prior to mounting. Anti-NPHS1 (R&D Systems Cat# AF4269) was used as primary antibody Secondary antibody was obtained from Molecular Probes (Thermo Fisher Scientific). Samples were mounted in 80,2% fructose with 0.5% (v/v) 1-thioglycerol. To generate 3D reconstructions of glomeruli, Z-series stacks were obtained from 300 µm kidney slices. Images were collected at 1µm intervals by using a Leica SP8 confocal microscope and deconvolved with Huygens Professional

software (Scientific Volume Imaging B.V., Hilversum, The Netherlands). We used image processing software from Leica Microsystems “Leica Application Suite X” for 3D reconstruction.

STED microscopy and slit diaphragm density quantification

STED xyz images (i.e., z stacks acquired along three directions: x, y, and z axes) were acquired by using an SP8 STED 3× confocal microscope (Leica Microsystems). Alexa Fluor tetramethyl rhodamine isothiocyanate (TRITC) secondary antibody was excited with a 555 nm tuned white light laser, and emission was collected from 565 to 605 nm. A 660-nm pulsed depletion laser was used with a gating between 0.7 and 6 ns. Images were acquired with Leica HC PL APO CS2 100×/1.40 oil STED white objective. Collected images were deconvolved with Huygens Professional software version 18.04. For the quantification of filtration slit coverage, z stacks of NPHS1 signal were acquired (at least 5 m thick). All the images of each z stack were merged, and the foot process length and the area of the field were determined using the ImageJ/Fiji macro, published by Butt et al. [14] and modified by Martin Klaus Five randomly selected areas for each glomerulus of at least five glomeruli per mouse were evaluated (n=4 mice/group).

Deep Learning morphometry analysis of WT1 and p57 stained immunohistochemistry slides

As mentioned previously, sections were stained with anti-mouse WT-1 and p57 antibody (1:200, Santa Cruz Biotechnology) by immunohistochemistry method. Subsequently, the slides were digitalized using a whole slide scanner (Aperio GT 450, Leica Biosystems, Wetzlar, Germany) with thanks to Marco Henrichs and Christoph Walz, Ludwig-Maximilans University, Institute of Pathology, Munich, Germany.

Especially in sclerotic slides, the WT1 staining was not highly specific to podocytes due to activated parrietal epithelial cells (see figure below). To this end, p57 staining was used for podocyte quantification [15].

To train and validate the algorithm, glomeruli, and podocytes were annotated by two trained and independent observers in eight randomly chosen kidney sections using QuPath [16]. Subsequently, pretrained U-Net based deep learning segmentation algorithms [17] were trained to segment kidney glomeruli and podocytes, respectively (see figure below). Obtained segmentation were filtered, and for the morphometric analysis only cell structures within the detected glomeruli were used. Glomerular area, podocyte count in each glomerulus, podocyte density within each glomerulus, and podocyte nuclear area in each glomerulus were computed.

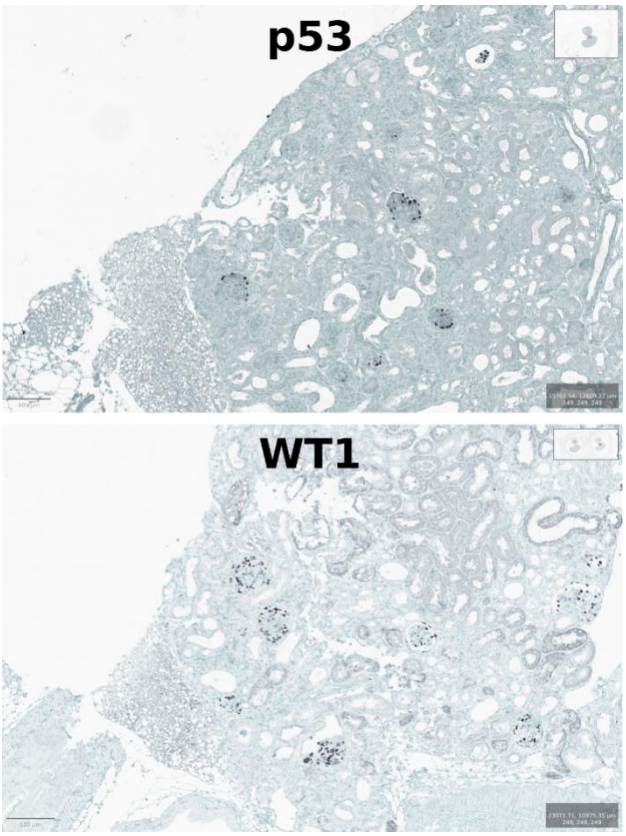

Exemplary section of a wt1 and p57 stained slide of a CKD-vehicle mouse with severe glomerulosclerosis.

Wildtype **CKD-vehicle**

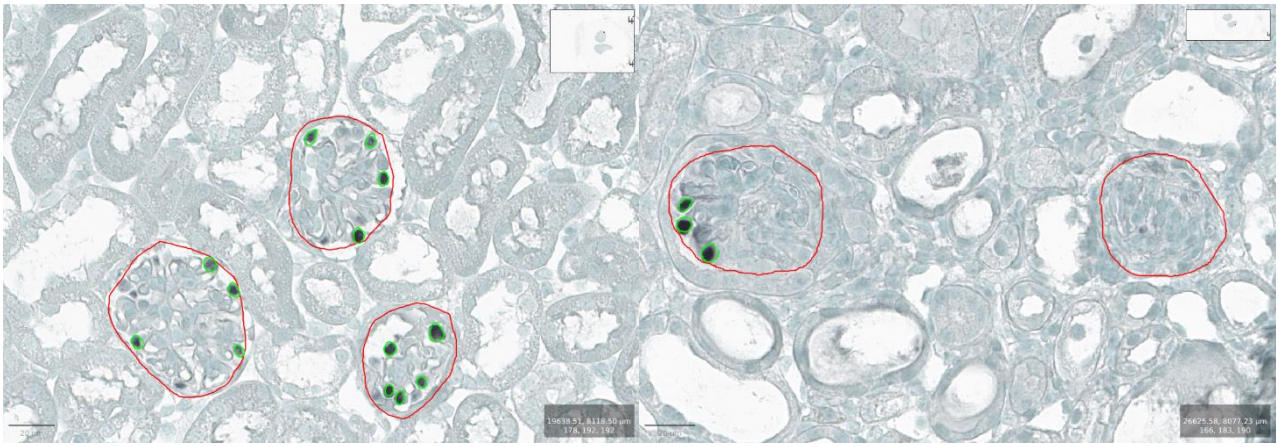

Exemplary section of a p57 stained whole slide image with the detected structures/cells by the deep learning segmentations: Glomerulus (red), Podocyte nuclei (green)

Supplementary file 5

Primers used for real-time qRT-PCR

Gene	Forward (5'-3')	Reverse (5'-3')
18s	GCAATTATTCCCCATGAACG	AGGGCCTCACTAAACCATCC
αSMA	CCTTCGTGACTACTGCCGAG	ATAGGTGGTTTCGTGGATGC
Fibronectin	GCCACCATTACTGGTCTGGA	GGTTGGTGATGAAGGGGGTC
TGFβ	CAACCCAGGTCCTTCCTAAA	GGAGAGCCCTGGATACCAAC
KIM-1	TCAGCTCGGGAATGCACAA	TGGTTGCCTTCCGTGTCTCT
NGAL	ATGTCACCTCCATCCTGG	GCCACTTGCACATTGTAG
IL18	AGAAAGCCGCCTCAAACCTT	TGTCTGATTCCAGGTCTCCATTT
TNFα	AGCCTCTTCTCATTCCTGCT	TAGACAAGGTACAACCCATC
TIMP2	GCAACAGGCGTTTTGCAATG	AGGTCCTTTGAACATCTTTATCTG
CCR5	GTCTACTTTCTCTTCTGGACTCC	CCAAGAGTCTCTGTTGCCTGCA
VCAM1	GCTATGAGGATGGAAGACTCTGG	ACTTGTGCAGCCACCTGAGATC
ICAM1	AAACCAGACCCTGGAACTGCAC	GCCTGGCATTTCAGAGTCTGCT
Il1b	TGGACCTTCCAGGATGAGGACA	GTTCATCTCGGAGCCTGTAGTG
IL6	TACCACTTCACAAGTCGGAGGC	CTGCAAGTGCATCATCGTTGTTC
Nephrin	CTGGGGGACAGTGGATTGAC	GGTCTGTGTCTTCAGGAGCC
Podocin	CTGTGAGTGGCTTCTTGTCCTC	CCTTTGGCTCTTCCAGGAAGCA
Col1α1	ACATGTTCAGCTTTGTGGAC	TAGGCCATTGTGTATGCAG

Supplementary Table 1

Evaluation of GFR in *Col4a3*-/- mice

Group (n=20)	GFR (µl/min)		
	Baseline (6 weeks)	7 weeks	10 weeks
CKD-veh	180.64 ± 32.11	146.95 ± 62.77	0.00 ± 0.00
CKD-RASi	187.61 ± 33.01	191.47 ± 44.36	54.46 ± 28.42
CKD-RASi/SGLT2i	187.25 ± 38.49	178.55 ± 30.48	55.43 ± 52.72
CKD-RASi/SGLT2i/MRA	185.27 ± 35.70	176.75 ± 39.21	125.40 ± 54.70

GFR, glomerular filtration rate; CKD, Chronic kidney disease

Supplementary Figure 1

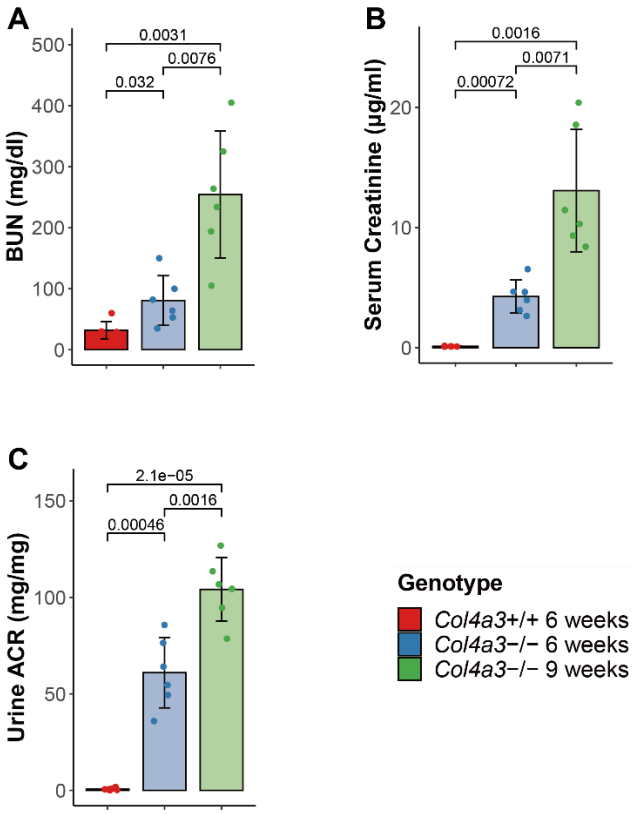

Supplementary figure 1: Assays for kidney function in *Col4a3*+/+ mice at 6 weeks and *Col4a3*-/- mice at 6 and 9 weeks.

(A) Levels of blood urea nitrogen (BUN). (B) Levels of serum creatinine. (C) Levels of urine albumin-creatinine ratio (UACR). All quantitative data are means ± SD.

Supplementary Figure 2

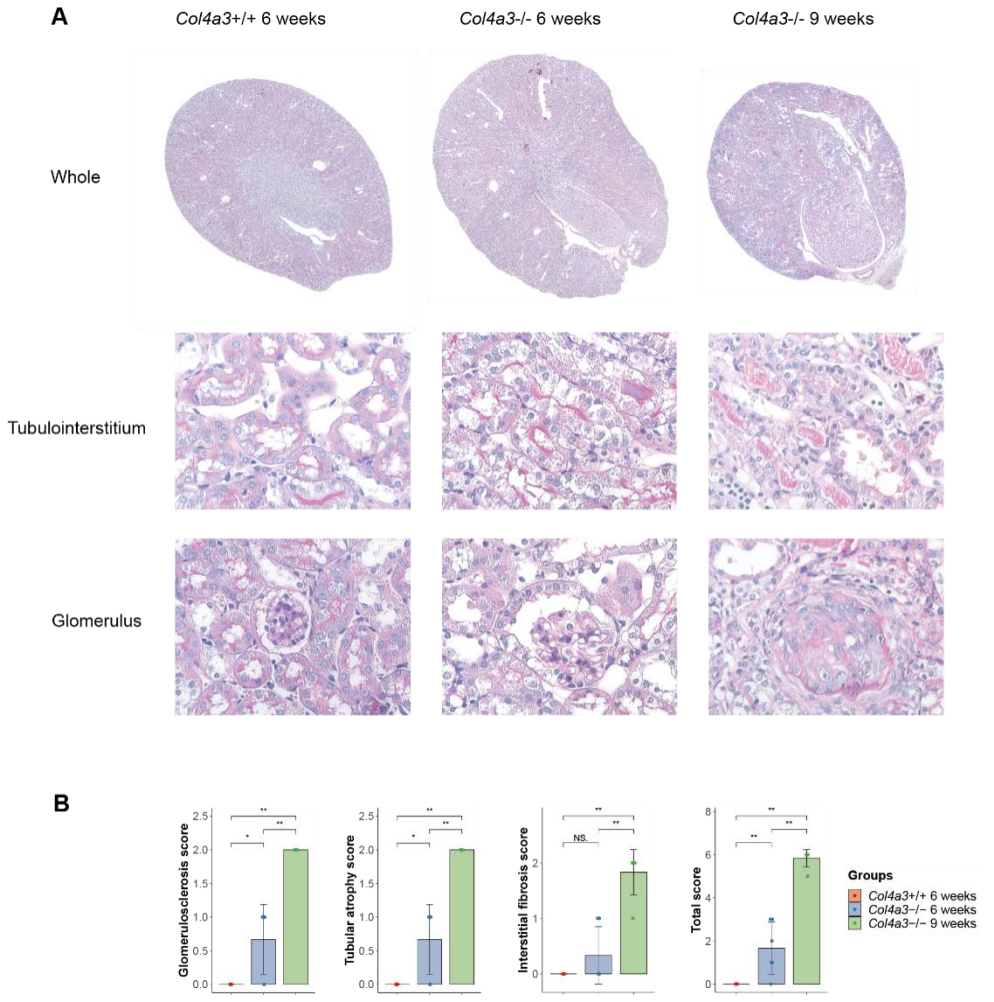

Supplementary figure 2: Tissue morphology and PAS staining quantitative assessment of scores from *Col4a3*+/+ mice at 6 weeks and *Col4a3*-/- mice at 6 and 9 weeks.

(A) PAS stained images from the whole kidney(above), tubules (middle) and glomerulus (below) are presented. (B) Kidney sections were independently scored for tubulointerstitial fibrosis, glomerulosclerosis and tubular atrophy. All quantitative data are means ± SD.*$p < 0.05$, **$p < 0.01$, NS. statistically not significant.

Supplementary Figure 3

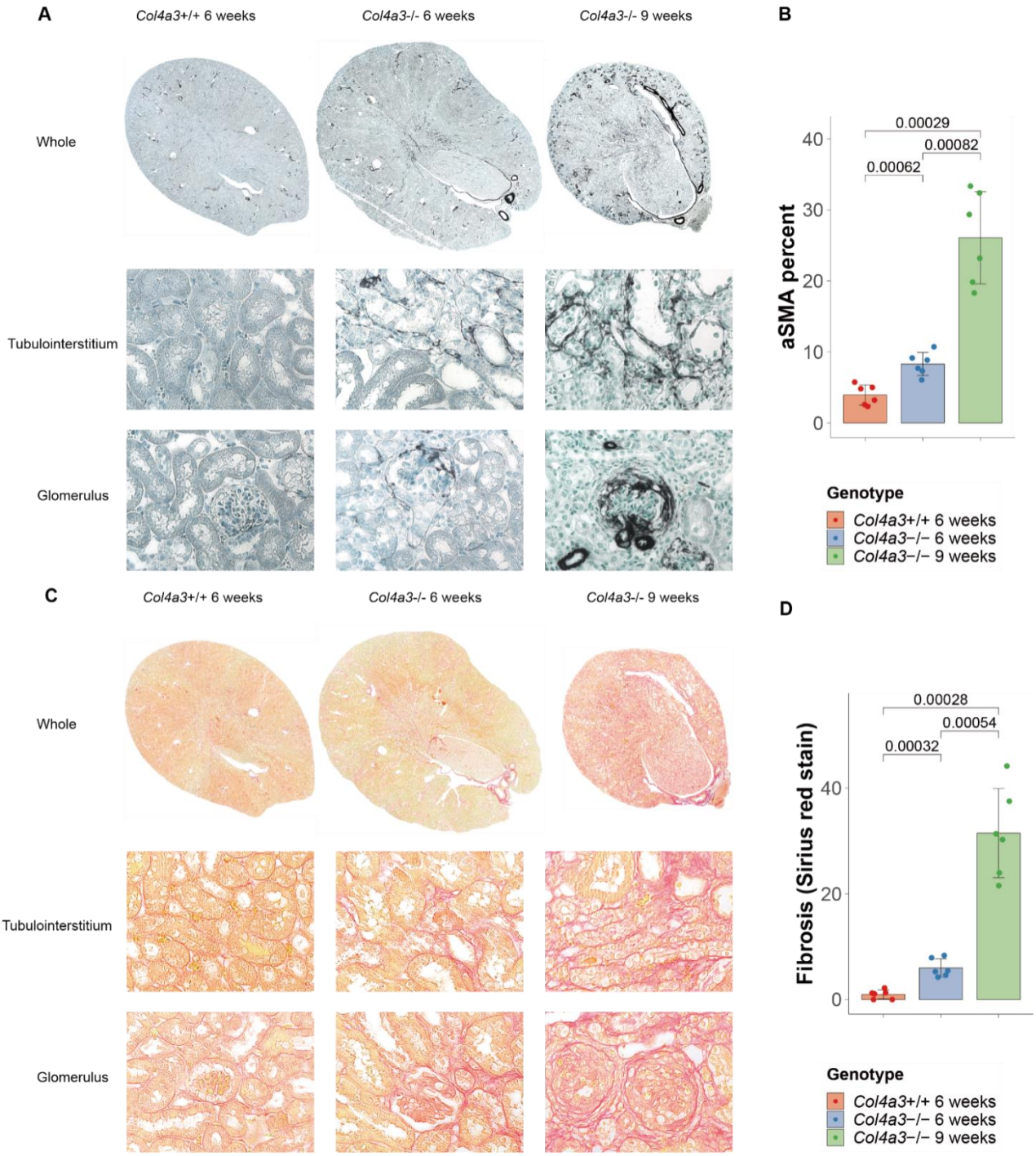

Supplementary figure 3: Tissue morphology and Sirius red and αSMA staining quantitative assessment of scores from *Col4a3*+/+ mice at 6 weeks and *Col4a3*-/- mice at 6 and 9 weeks.

(A) αSMA stained images from the whole kidney (above), tubules (middle) and glomerulus (below) are presented. (B) Kidney sections were independently scored for αSMA staining positive area. (C) Sirius red stained images from the whole kidney(above), tubules (middle) and glomerulus (below) are presented. (D) Kidney sections were independently scored for Sirius red positive area. All quantitative data are means ± SD.

Supplementary Figure 4

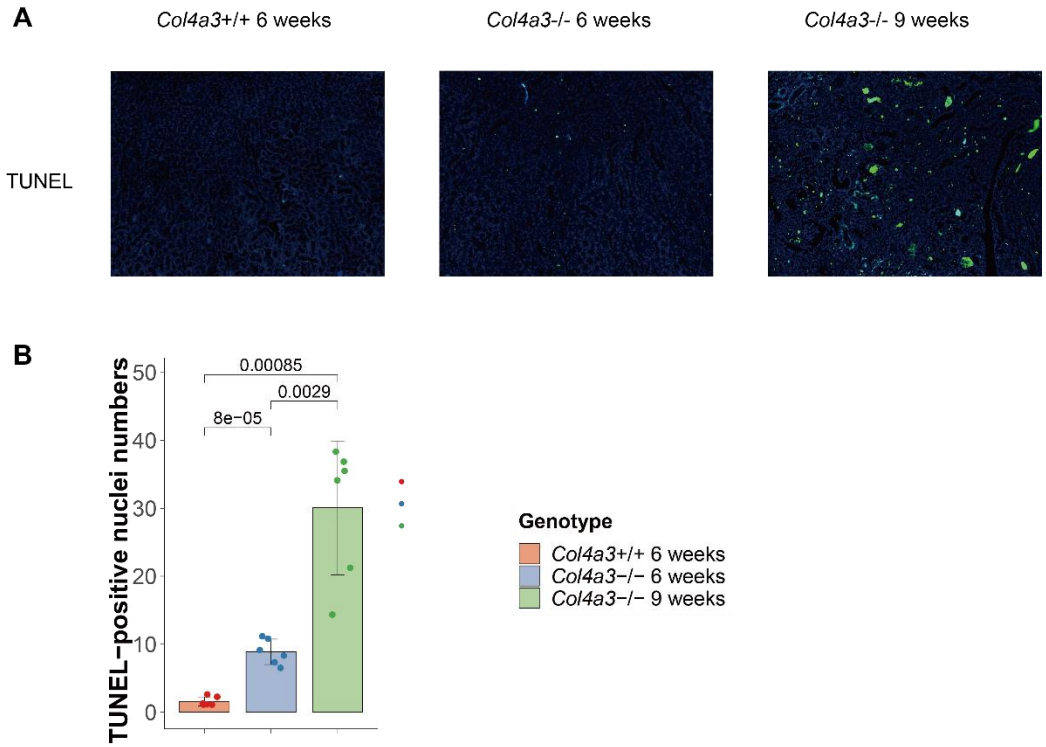

Supplementary figure 4: TUNEL staining quantitative assessment of scores from *Col4a3*+/+ mice at 6 weeks and *Col4a3*-/- mice at 6 and 9 weeks.

(A) Representative TUNEL stained images from the glomerulus are presented. (B) Kidney sections were independently scored for TUNEL-positive nuclei numbers. All quantitative data are means ± SD.

Supplementary Figure 5

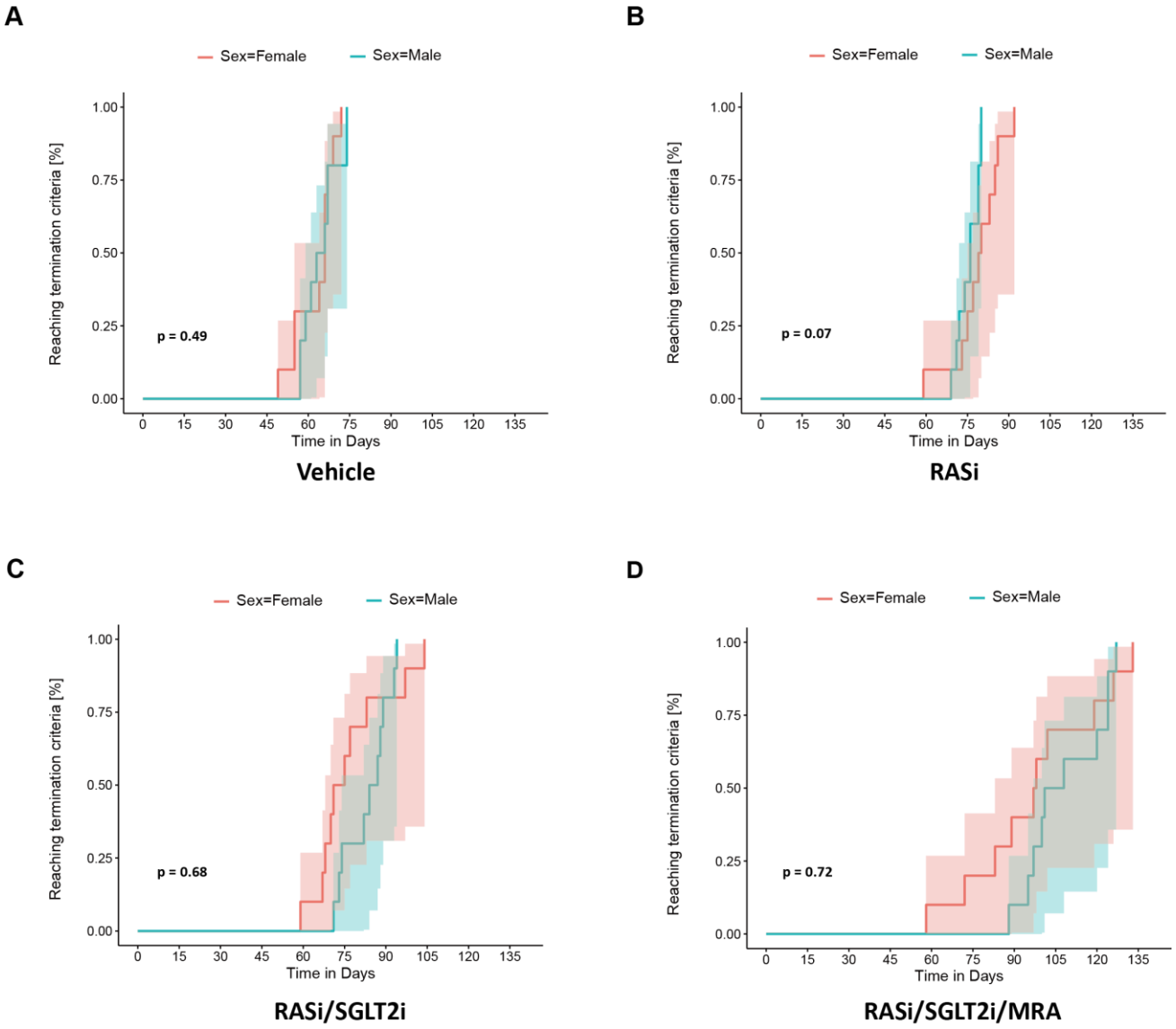

Supplementary figure 5: Subgroup of lifespan by sex.

(A) Sex differences in vehicle group. (B) Sex differences in RASi group. (C) Sex differences in RASi/SGLT2i group. (D) Sex differences in RASi/SGLT2i/MRA group. All quantitative data are means ± SD.

Supplementary Figure 6

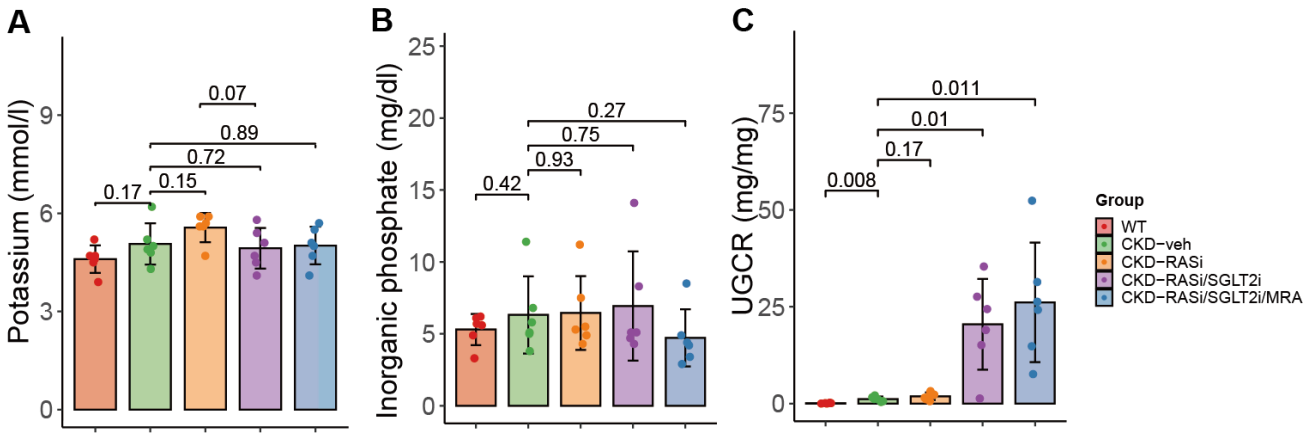

Supplementary figure 6: Effects of RASi, RASi/SGLT2i, and RASi/SGLT2i/MRA treatments on potassium and inorganic phosphate serum levels and urine glucose/creatinine ratio (UGCR) in Col4a3-/- mice.

(A) The serum levels of potassium at 8.5 weeks. (B) The serum level of inorganic phosphate at 8.5 weeks. (C) The UGCR level at 8.5 weeks. All quantitative data are means ± SD.

Supplementary Figure 7

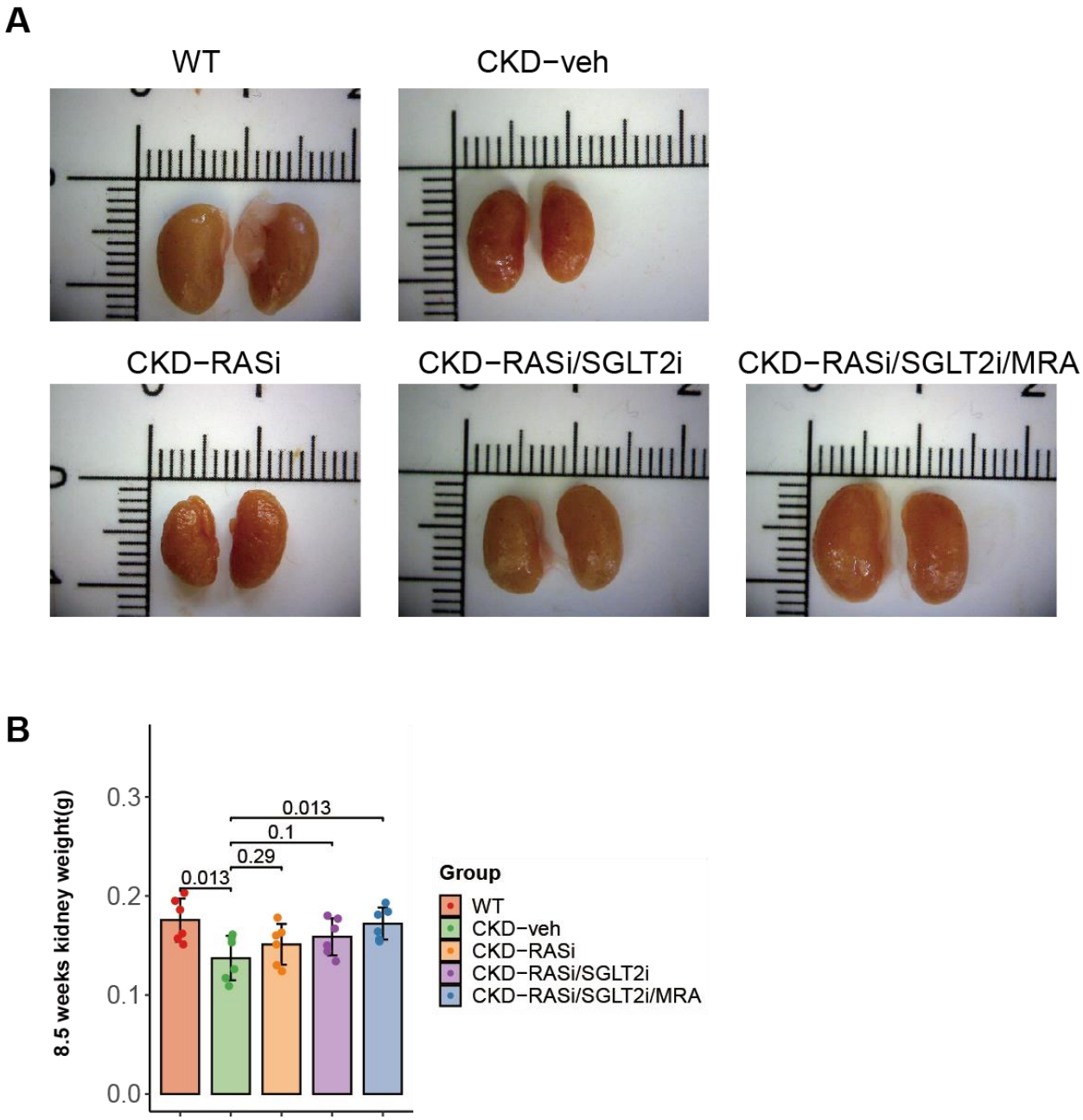

Supplementary figure 7: Triple therapy prevented kidney atrophy to the level of wildtype controls.

(A) Representative 8.5 weeks kidney images. (B) 8.5 weeks kidney weight. All quantitative data are means ± SD.

Supplementary Figure 8

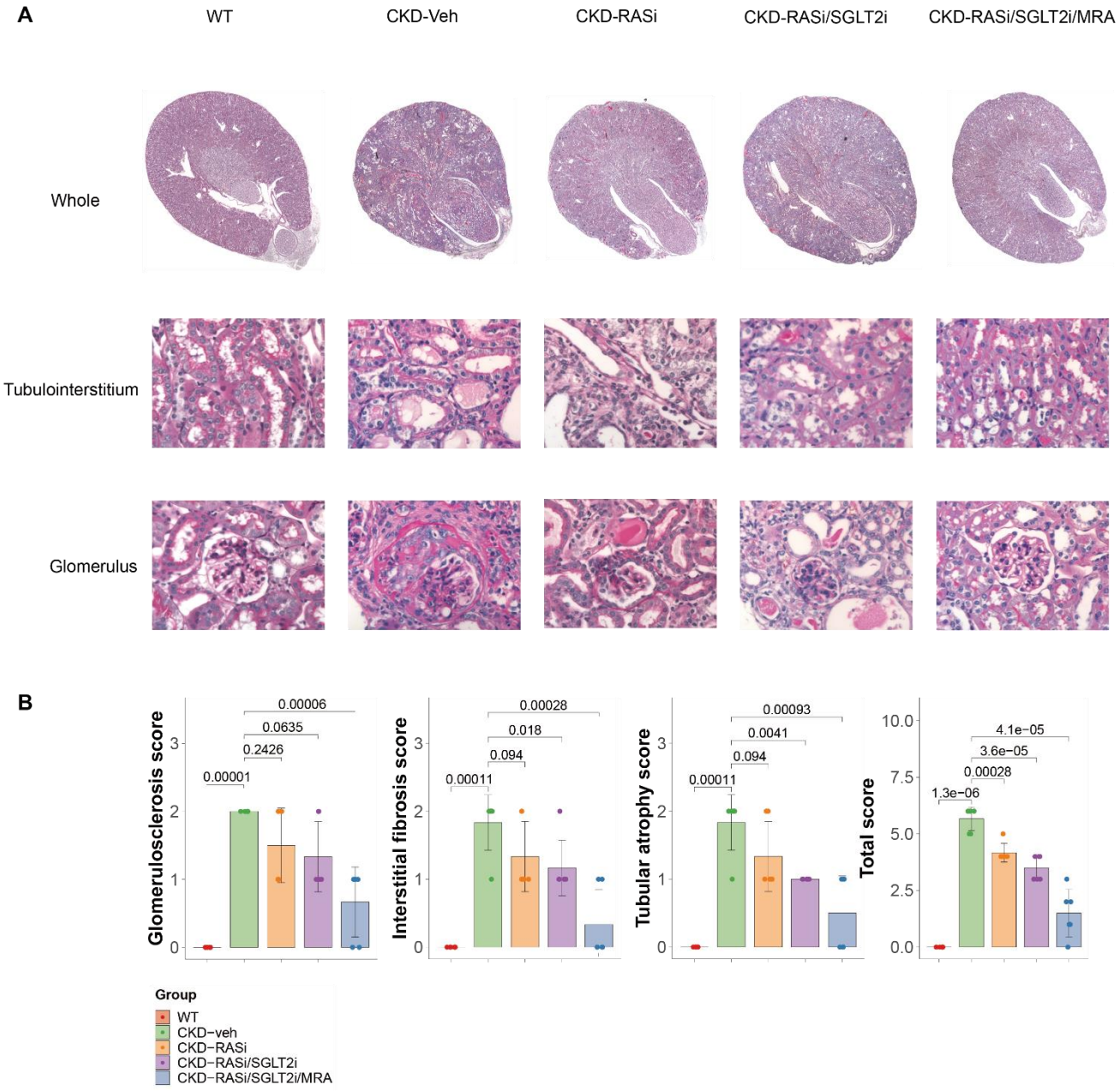

Supplementary figure 8: Tissue morphology and PAS staining quantitative assessment of scores from *Col4a3*-/- mice in WT, Veh, RASi, RASi/SGLT2i, and RASi/SGLT2i/MRA groups

(A) Representative PAS-stained images from the whole kidney, tubules and glomerulus are presented. (B) Kidney sections were independently scored for tubulointerstitial fibrosis, glomerulosclerosis and tubular atrophy. All quantitative data are means ± SD. Images are shown at the magnification of 200x and 400x

Supplementary Figure 9

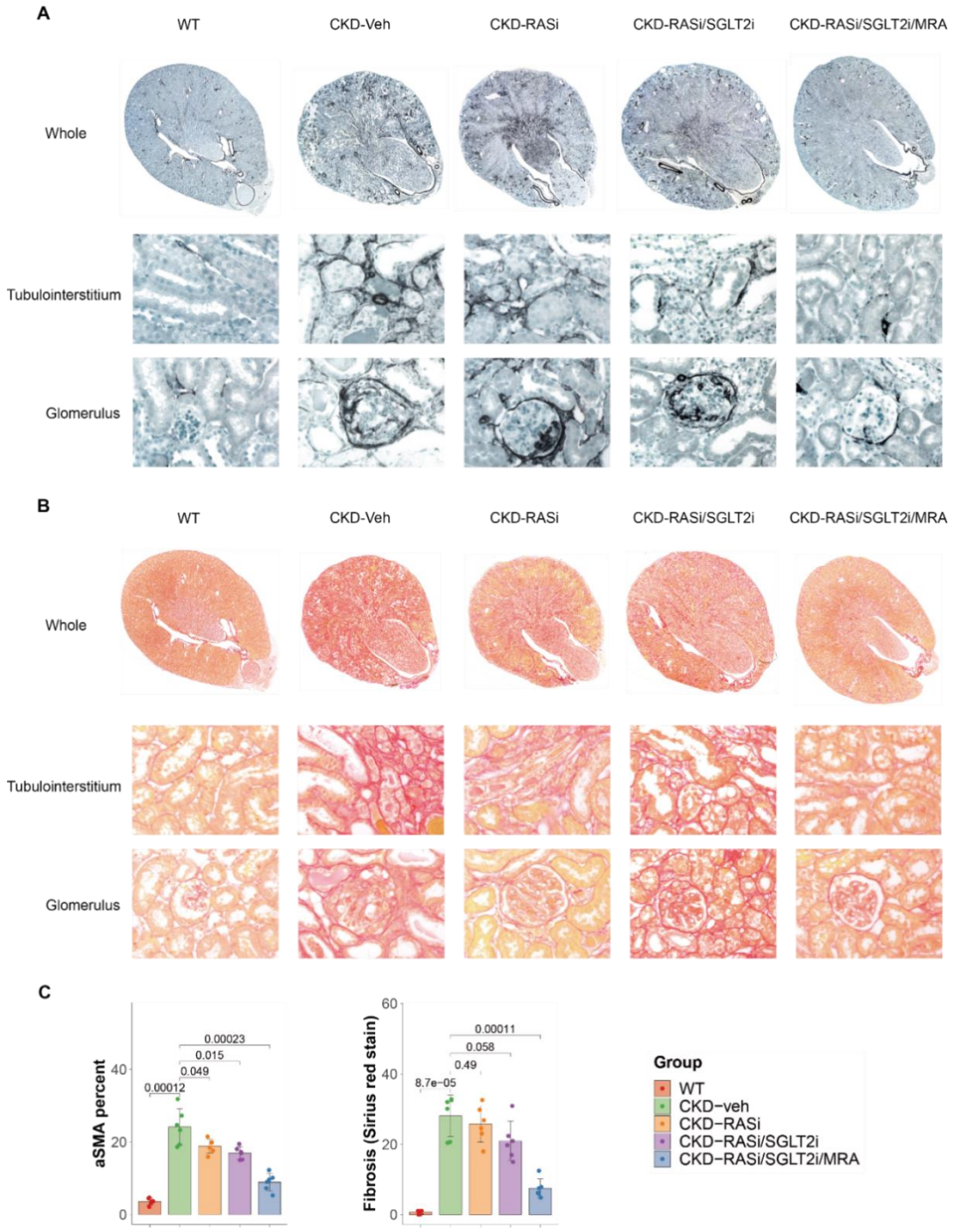

Supplementary figure 9: Tissue morphology and αSMA and Picro-Sirius red staining quantitative assessment of scores from *Col4a3*-/- mice in WT, Veh, RASi, RASi/SGLT2i, and RASi/SGLT2i/MRA groups

(A, B) Representative αSMA and Picro-Sirius red stained images from the whole kidney, tubules and glomerulus. (C) Kidney sections were independently scored for αSMA positive percent and Picro-Sirius red positive percent. All quantitative data are means ± SD. Images are shown at the magnification of 200x and 400x.

Supplementary Figure 10

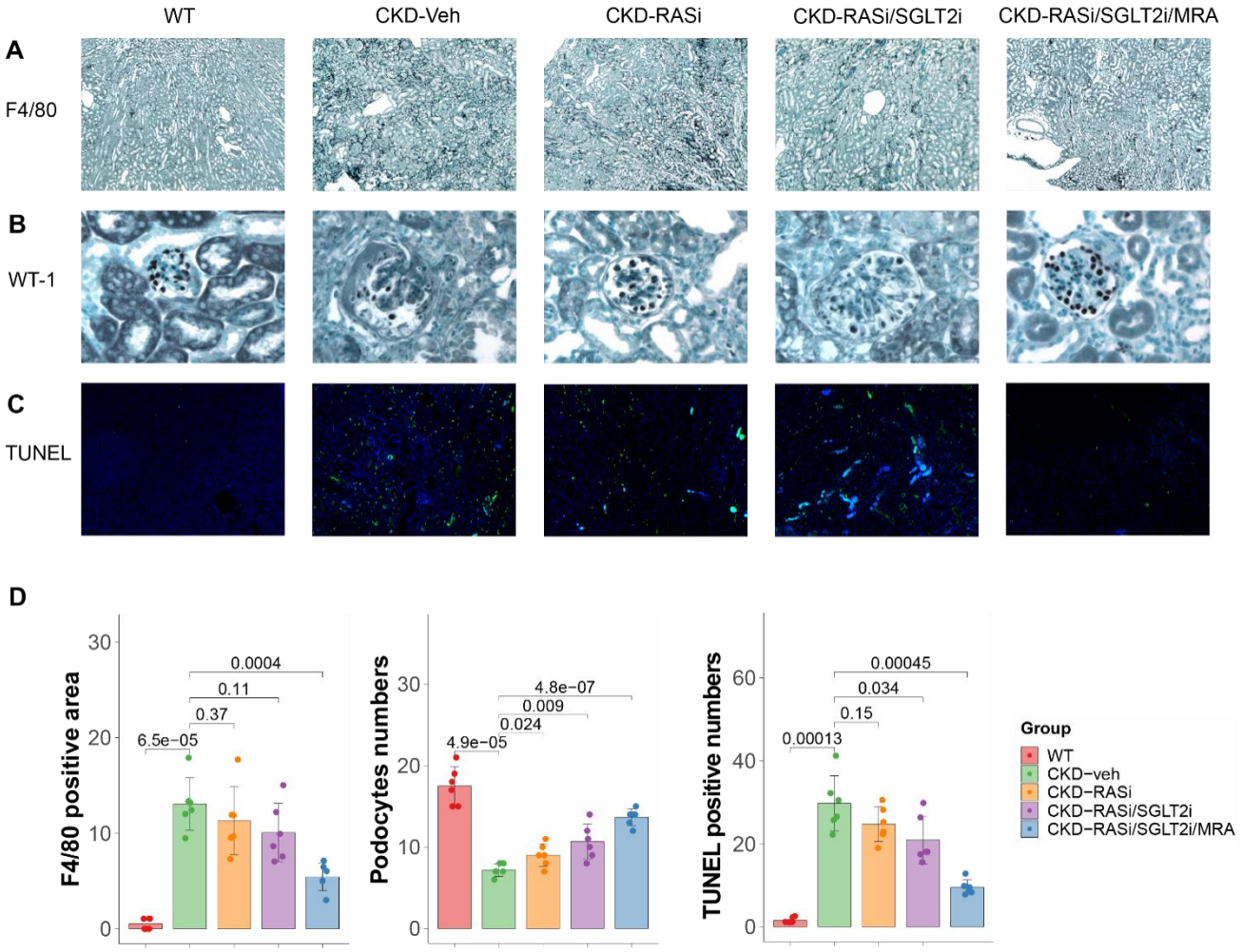

Supplementary figure 10: Tissue morphology and F4/80, WT-1, and TUNEL staining quantitative assessment of scores from *Col4a3*-/- mice in WT, veh, RASi, RASi/SGLT2i, and RASi/SGLT2i/MRA groups

(A) Representative F4/80-stained images from junction of kidney cortex and medulla are presented. (B) Representative WT1-stained images from the kidney glomerulus are presented. (C) Representative TUNEL stained images from the kidneys are presented. (D) Kidney sections were independently scored for F4/80 positive percent, podocytes numbers, and the number of TUNEL-positive nuclei per 100 tubules. All quantitative data are means ± SD. Images are shown at the magnification of 200x and 400x.

Supplementary Figure 11

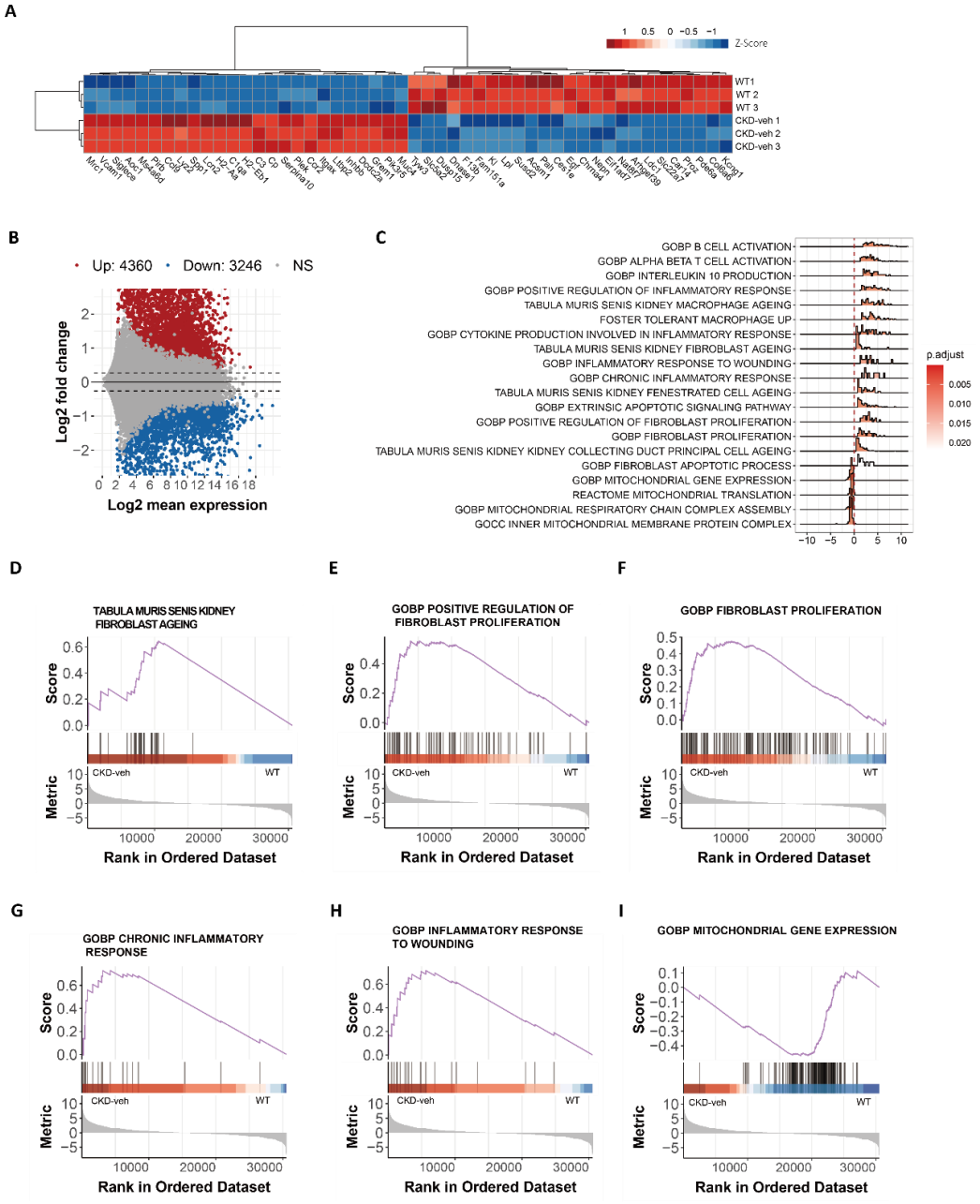

Supplementary figure 11: Bulk RNA-seq on kidney of Veh-treated Alport and wildtype mice

(A) The heatmap presents the biological replicates of the top genes with differing expression levels between the Veh-treated *Col4a3*-/- and wildtype mice. A heatmap and dendrogram were used to display the differentially expressed genes' z-scores of normalized counts. (B) An MA plot was also created to display the shrink log2 fold change between kidney of the Veh-treated *Col4a3*-/- and wildtype mice. Genes differentially regulated in a significant manner, as indicated by an adjusted p-value, are labeled either in red or blue. (C) The density ridge plot shows the gene expression distribution of core-enriched genes in enriched gene sets, with gradient color indicating adjusted *p*-values using the Benjamini-Hochberg method. (D-I) The selected enrichment plots from the GSEA analysis based on the gene enrichment profiles of the Veh-treated *Col4a3*-/- versus wildtype mice. The plots highlight the enrichment for transcriptional signatures related to inflammation, fibrosis, and mitochondrial function.

Supplementary Figure 12

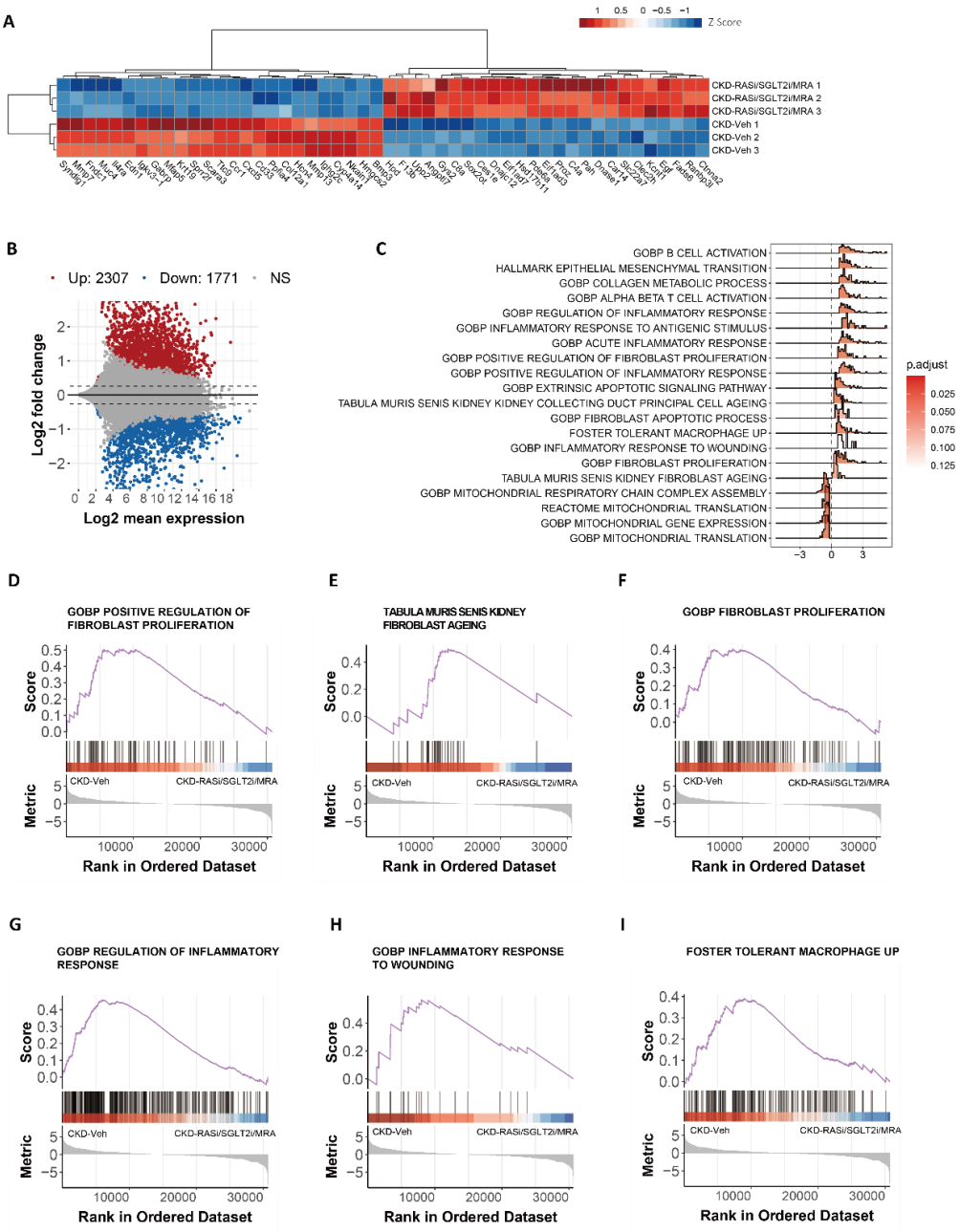

Supplementary figure 12: Bulk RNA-seq on kidney of Alport mice on triple therapy versus vehicle

(A) The heatmap presents the biological replicates of the top genes with differing expression levels between the *Col4a3*-/- mice on triple therapy versus vehicle. A heatmap and dendrogram were used to display the differentially expressed genes' z-scores of normalized counts. (B) An MA plot was also created to display the shrink log2 fold change between kidneys of the vehicle and triple therapy-treated *Col4a3*-/- mice. Genes that are found to be significant in differential expression testing, as indicated by an adjusted *p*-value, are labeled either in red or blue. (C) The density ridge plot shows the gene expression distribution of core-enriched genes in enriched gene sets, with gradient color indicating adjusted *p*-values using the Benjamini-Hochberg method. (D-I) The selected enrichment plots from the GSEA analysis based on the gene enrichment profiles of the vehicle and triple therapy. The plots highlight the enrichment for transcriptional signatures related to inflammation, fibrosis, and mitochondrial function

Supplementary Figure 13

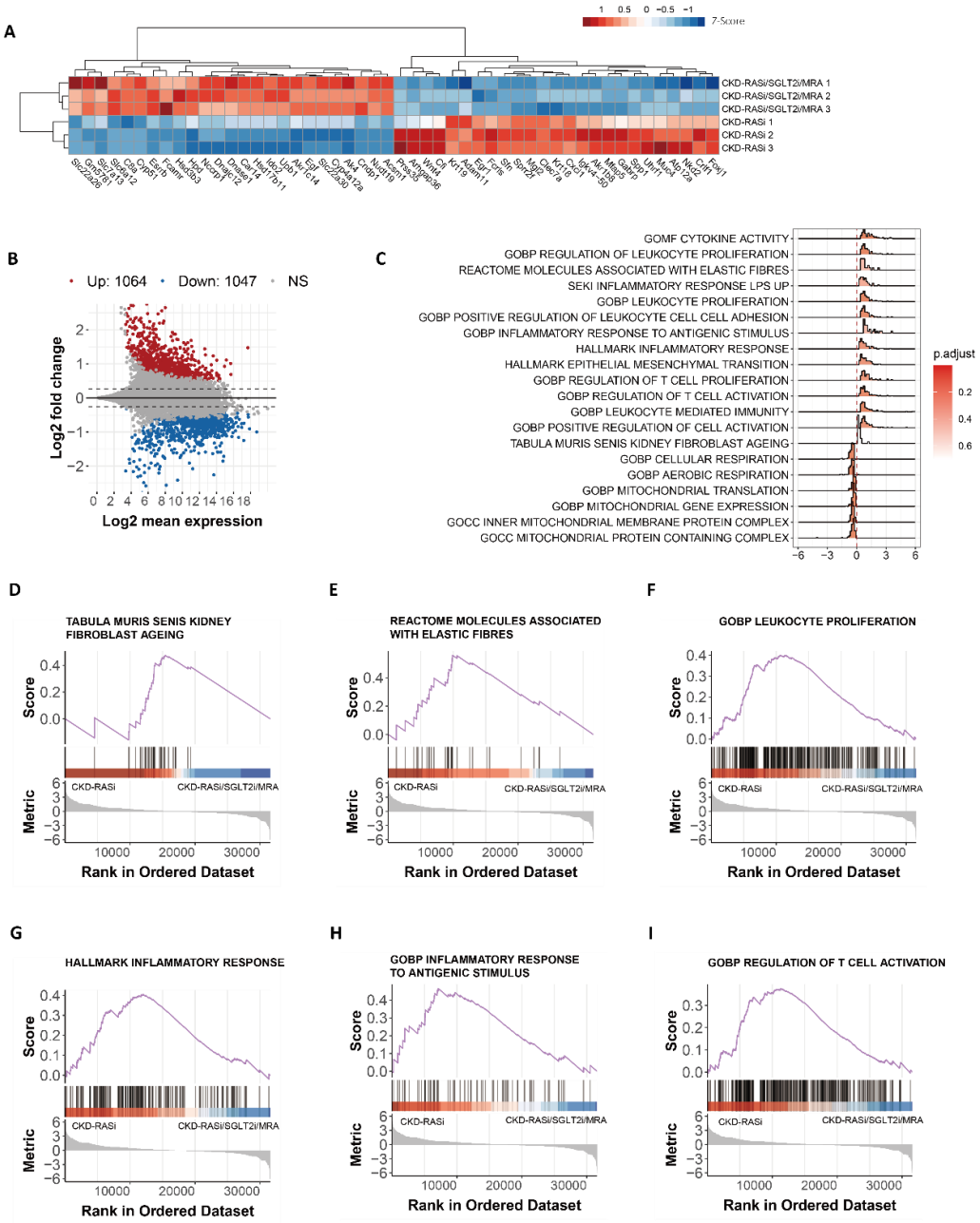

Supplementary figure 13: Bulk RNA-seq on kidney of Alport mice on triple versus monotherapy

(A) The heatmap presents the biological replicates of the top genes with differing expression levels between the *Col4a3*-/- mice on triple versus mono therapy. A heatmap and dendrogram were used to display the differentially expressed genes' z-scores of normalized counts. (B) An MA plot was also created to display the shrink log2 fold change between kidneys of the mono and triple therapy-treated *Col4a3*-/- mice. Genes that are found to be significant in differential expression testing, as indicated by an adjusted *p*-value, are labeled either in red or blue. (C) The density ridge plot shows the gene expression distribution of core-enriched genes in enriched gene sets, with gradient color indicating adjusted *p*-values using the Benjamini-Hochberg method. (D-I) The selected enrichment plots from the GSEA analysis based on the gene enrichment profiles of the mono and triple therapy. The plots highlight the enrichment for transcriptional signatures related to inflammation, fibrosis, and mitochondrial function

Supplementary Figure 14

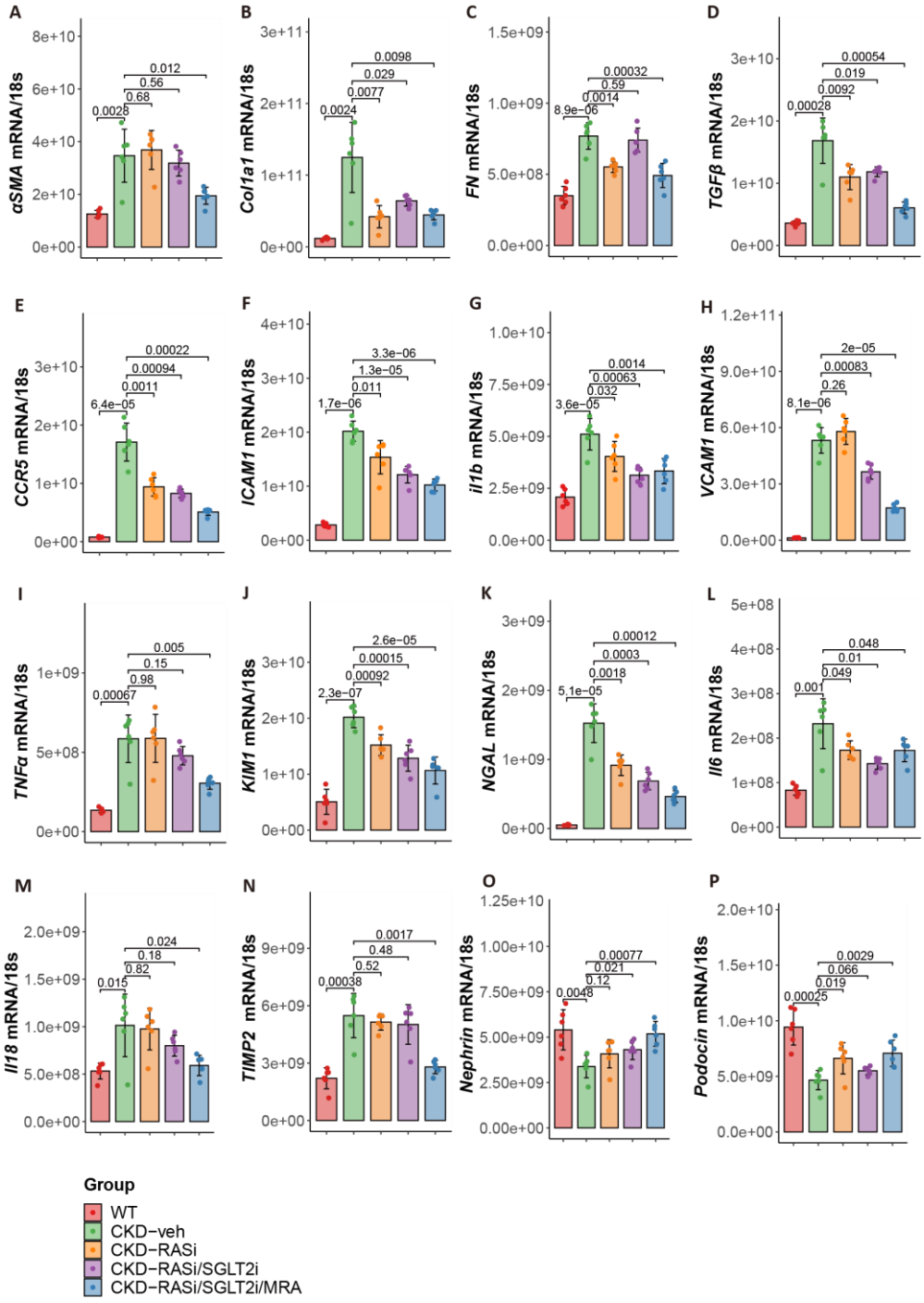

Supplementary figure 14: Relative kidney mRNA expression of kidney fibrosis, inflammation, injury, and podocyte markers

Gene expression was analyzed by RT-qPCR for fibrosis makers (A) *αSMA* (B) *Col1α1* (C) *FN* (D) *TGFβ,* inflammation makers (E) *CCR5* (F) *ICAM1* (G) *Il1β* (H) *VCAM1,* injury makers (I) *TNFα* (J) *KIM1* (K) *NGAL* (L) *Il6* (M) *Il18* (N) *TIMP2,* and podocyte makers (O) *Nephrin* (P) *Podocin.* All quantitative data are means ± SD

Supplementary Reference

1. Gross O, Beirowski B, Koepke ML, et al. Preemptive ramipril therapy delays renal failure and reduces renal fibrosis in COL4A3-knockout mice with Alport syndrome. *Kidney Int* 2003; **63**(2): 438-46.
2. Tomita I, Kume S, Sugahara S, et al. SGLT2 Inhibition Mediates Protection from Diabetic Kidney Disease by Promoting Ketone Body-Induced mTORC1 Inhibition. *Cell Metab* 2020; **32**(3): 404-19 e6.
3. Droebner K, Pavkovic M, Grundmann M, et al. Direct Blood Pressure-Independent Anti-Fibrotic Effects by the Selective Nonsteroidal Mineralocorticoid Receptor Antagonist Finerenone in Progressive Models of Kidney Fibrosis. *Am J Nephrol* 2021; **52**(7): 588-601.
4. Barrera-Chimal J, Estrela GR, Lechner SM, et al. The myeloid mineralocorticoid receptor controls inflammatory and fibrotic responses after renal injury via macrophage interleukin-4 receptor signaling. *Kidney Int* 2018; **93**(6): 1344-55.
5. Motrapu M, Swiderska MK, Mesas I, et al. Drug Testing for Residual Progression of Diabetic Kidney Disease in Mice Beyond Therapy with Metformin, Ramipril, and Empagliflozin. *J Am Soc Nephrol* 2020; **31**(8): 1729-45.
6. Schreiber A, Shulhevich Y, Geraci S, et al. Transcutaneous measurement of renal function in conscious mice. *Am J Physiol Renal Physiol* 2012; **303**(5): F783-8.
7. Kim D, Paggi JM, Park C, Bennett C, Salzberg SL. Graph-based genome alignment and genotyping with HISAT2 and HISAT-genotype. *Nat Biotechnol* 2019; **37**(8): 907-15.
8. Li H, Handsaker B, Wysoker A, et al. The Sequence Alignment/Map format and SAMtools. *Bioinformatics* 2009; **25**(16): 2078-9.
9. Liao Y, Smyth GK, Shi W. featureCounts: an efficient general purpose program for assigning sequence reads to genomic features. *Bioinformatics* 2014; **30**(7): 923-30.
10. Gaidatzis D, Burger L, Florescu M, Stadler MB. Analysis of intronic and exonic reads in RNA-seq data characterizes transcriptional and post-transcriptional regulation. *Nat Biotechnol* 2015; **33**(7): 722-9.
11. Yu G, Wang LG, Han Y, He QY. clusterProfiler: an R package for comparing biological themes among gene clusters. *OMICS* 2012; **16**(5): 284-7.
12. Holscher DL, Bouteldja N, Joodaki M, et al. Next-Generation Morphometry for pathomics-data mining in histopathology. *Nat Commun* 2023; **14**(1): 470.
13. Bouteldja N, Klinkhammer BM, Bulow RD, et al. Deep Learning-Based Segmentation and Quantification in Experimental Kidney Histopathology. *J Am Soc Nephrol* 2021; **32**(1): 52-68.
14. Butt L, Unnersjo-Jess D, Hohne M, et al. A molecular mechanism explaining albuminuria in kidney disease. *Nat Metab* 2020; **2**(5): 461-74.
15. Taniguchi Y, Pippin JW, Hagmann H, et al. Both cyclin I and p35 are required for maximal survival benefit of cyclin-dependent kinase 5 in kidney podocytes. *Am J Physiol Renal Physiol* 2012; **302**(9): F1161-71.
16. Bankhead P, Loughrey MB, Fernandez JA, et al. QuPath: Open source software for digital pathology image analysis. *Sci Rep* 2017; **7**(1): 16878.

17. Zimmermann M, Klaus M, Wong MN, et al. Deep learning-based molecular morphometrics for kidney biopsies. *JCI Insight* 2021; **6**(7).